Reconciling ultra-emitter detections from two aerial hyperspectral imaging surveys in the Permian Basin

Yuanlei Chen[1*], Evan D. Sherwin[1], Erin B. Wetherley[2], Petr V. Yakovlev[2], Elena S.F. Berman[2], Brian B. Jones[2], Benjamin Hmiel[3,4], David R. Lyon[3,5], Riley M. Duren[6,7,8], Daniel H. Cusworth[6], Adam R. Brandt[1]

[1] Department of Energy Science and Engineering, Stanford University, Stanford, California, US

[2] Insight M, Inc., Sunnyvale, California, US

[3] Environmental Defense Fund, Austin, Texas, US

[4] Now at: Colorado Department of Public Health and Environment, Denver, Colorado, US

[5] Now at: Environmental Protection Agency, Washington, D.C., US

[6] Carbon Mapper, Inc., Pasadena, California, US

[7] Arizona Institutes for Resilience, University of Arizona, Tucson, Arizona, US

[8] Jet Propulsion Laboratory, California Institute of Technology, Pasadena, California, US

*yuliac@stanford.edu

Abstract

Reducing methane emissions from oil and gas operations is key to minimizing the climate impact of fossil fuels. Two comprehensive aerial studies in 2019 in the Permian Basin revealed excess emissions compared to official estimates. Although both studies suggested high emissions, the estimates from the two aerial surveys seemed to differ greatly: one study measured 153 (+12/-10, 95% CI) metric tons of methane per hour (t/h), or 7.5% (+0.6%/-0.5%) of gross gas production from aerially detectable point sources in the New Mexico Permian Basin, while the other estimated 246±96 t/h, or 2.7±0.9% of the gross gas production in the larger Texas and New Mexico portions of the Permian Basin. This paper explores causes of this apparent discrepancy by comparing observations of ultra-emitters (>500 kg/h) detected by each survey across a large, spatially overlapping survey region. We account for differences in sensor performance, study scope and design, and data processing practices of the two aerial studies. By aligning approaches, we reconcile the mean ultra-emitter emissions estimates in the applicable overlapping survey area with relative differences as low as 13%, down from 176% for the two full estimates before alignments. T-tests show a p-value increase from 1.2×10^{-5} to 0.182, indicating that the differences between the two aerial-based estimates are not statistically significant after reconciliation. The apparent discrepancy between the studies as published is due to sub-basin level heterogeneous emissions, differing sensor minimum detection limits, and missed ultra-emitters over 1 t/h due to infrequent surveys. Temporal variability in emissions raises an estimation challenge, but this can be mitigated with repeated comprehensive surveys. This work points to methods to improve comparability and repeatability of future estimates, and offers methods to ensure that measured assets are representative of the full area of interest.

Keywords: methane emissions, aerial survey, remote sensing, hyperspectral imaging, oil and gas

Introduction

Methane, the primary constituent of natural gas, is the second most important anthropogenic greenhouse gas. US natural gas and petroleum systems were estimated to emit 32% of total US 2020 anthropogenic methane emissions in the official US Greenhouse Gas Inventory (GHGI) (U.S. Environmental Protection Agency 2023).

Independent studies suggest that the GHGI underestimates oil and gas methane emissions (Alvarez *et al* 2018; Brandt, Heath, and Cooley 2016), largely due to the outdated data sources used in the GHGI and due to bottom-up methods that systematically exclude infrequent large emissions (so-called "super-emitters") (Brandt, Heath, and Cooley 2016; Rutherford *et al* 2021).

One way to mitigate the bias resulting from missing super-emitters in measurement-based studies is to enlarge the sample size so that a sufficient number of super-emitters enter the sample (Sherwin *et al* 2024; Johnson *et al* 2023). Super-emitting events are infrequent and therefore adequately characterizing them can require sample sizes much larger than is feasible with ground campaigns. Remote sensing is a more feasible approach because it can detect and quantify emissions over an extensive area with reasonable costs and time (Johnson *et al* 2021a), and can detect emissions from all sites regardless of ownership.

Recently, basin-wide comprehensive surveys that measure methane point sources from oil and gas facilities have been made possible by hyperspectral aerial imaging surveys (Duren *et al* 2019; Frankenberg *et al* 2016; Cusworth *et al* 2022; Chen, Sherwin *et al* 2022; Cusworth *et al* 2021). These comprehensive surveys can generate estimates for sources large enough to be seen via aerial imaging at a regional level.

In 2019, two hyperspectral aerial imaging surveys were deployed in the Permian Basin (Chen, Sherwin *et al* 2022; Cusworth *et al* 2021). At that time, the Permian Basin had become the largest and fastest-growing oil and gas-producing basin in the US. From 2015 to 2020, oil production in the Permian Basin grew from 1.5 million barrels per day (mmb/d) to 4.2 mmb/d, and gas production went up from 5.2 billion cubic feet per day (bcf/d) to 16.8 bcf/d, or 176% and 226% growth respectively (Enverus 2023). With the rapid production growth, the Permian Basin has also been identified as a major methane emitting region in recent years by satellite-based observations (Schneising *et al* 2020; Zhang *et al* 2020; Shen *et al* 2022; Irakulis-Loitxate *et al* 2021; McNorton *et al* 2022; Varon *et al* 2023), tower-based sensor networks (Lyon *et al* 2021; Barkley *et al* 2023), ground surveys (Robertson *et al* 2020), and more recent hyperspectral aerial survey by MethaneAIR (MethaneSAT 2023; MethaneSAT 2024).

However, emission estimates from these two comprehensive 2019 aerial studies of the Permian Basin do not seem to agree. Using data from an aerial survey conducted by Insight M that covered over 90% of oil and gas facilities in the New Mexico Permian Basin, Chen, Sherwin et al. estimate total directly measured methane emissions in their survey area at 153 (+12/-10, 95% CI) metric tons of methane per hour (t/h), 7.5% (+0.6%/-0.5%) of the methane in natural gas produced in the survey area during their survey time from October 2018 to January 2020.

In a shorter time window from September to November 2019, Cusworth et al. used two hyperspectral sensors – the Next-Generation Airborne Visible/Infrared Imaging Spectrometer (AVIRIS-NG) and the Global Airborne Observatory (GAO) – to sample much of the Permian Basin, including a section that overlaps with the Insight M survey (Cusworth *et al* 2021). The Cusworth et al. survey quantified total emissions from large point sources at 246±79 t/h (Cusworth *et al* 2022), roughly 2.7±0.9% of gross gas production in their full survey area (Enverus 2023). Note that the underlying methods to account for intermittency differ between the two aerial studies – if Cusworth et al. apply the intermittency accounting method used in Chen, Sherwin et al., total emissions would be estimated at 449 (-16/+18) t/h, bringing up the production loss rate to 4.1±0.2%. In a third study of the Permian basin which will not be compared in detail here, MethaneAIR surveyed the Delaware Sub-basin in 2021 and identified 91 t/h of emissions in the area, similar to what Cusworth et al. found in the Delaware part of their survey area (MethaneSAT 2023; Sherwin *et al* 2024).

One obvious difference between the Insight M and the Cusworth et al. studies is the difference in regional coverage. If we only compare the measurements from the overlapping survey area of the two studies, the Insight M study estimates 142 (+12/-10) t/h of methane emissions or 7.2% (+0.6%/-0.5%) of gas production and the Cusworth et al. estimates 79 (+9/-7) t/h or 3.6%±0.4% of gas production. Although both numbers are much larger than the 1.0% estimate by the 2020 GHGI (Sherwin *et al* 2024), the discrepancies in the two aerial surveys remain.

Given the superficial similarity between these two surveys, why are these two results so different within the same geographic area? If aerial surveys are to form a basis for updating our estimates of total emissions from a region or an operator, we need to understand the sources of the discrepancy. This study compares and reconciles the results from these two aerial surveys of the Permian Basin, providing insights into nuances of estimating emissions from large-scale aerial surveys. We also highlight best practices for planning future aerial surveys to inform emissions at a regional level.

Methods

From September to November 2019, Cusworth et al. used the AVIRIS-NG and the GAO airplanes to map super-emitters in the Permian Basin, finding 3067 methane emission incidences from 1756 distinct sources associated with upstream and midstream oil and gas infrastructure. GAO was deployed to survey the light blue polygons in Figure 1 and covered the entirety of the two light blue polygons at least once. These polygons contain production infrastructure that accounted for 91% of gas production and 92% of oil production in the Permian Basin during the campaign (Sherwin *et al* 2024). During approximately the same time, AVIRIS-NG was used to image assets in the much smaller purple polygons at least seven times (Cusworth *et al* 2021). The purple polygons are areas of large production volume, and the repeated coverage increases the temporal resolution in core production areas and aim to explore the intermittency of aerially visible large sources.

GAO and AVIRIS-NG are installed with identical imaging spectrometers but were deployed at different altitudes in these surveys. GAO was deployed at ~5,300 m above mean sea level and surveyed a wider extent of the Permian Basin and the AVIRIS-NG instrument was flown at ~8,500 m to rapidly and repeatedly survey the core production region (purple polygons) of the Permian Basin (Cusworth *et al* 2021).

Over a longer time period from October 2018 to January 2020, Insight M conducted an aerial methane survey using its proprietary LeakSurveyor, a hyperspectral imaging system that is mounted on an airplane deployed at ~900 m above ground (Kairos Aerospace 2019). The Insight M survey focused on the New Mexico Permian Basin (orange polygon in Figure 1), where the state government was drafting flaring and venting regulations at the time of the survey in response to the unprecedented oil and gas production in the state (New Mexico 2021). The Insight M survey made an average of four repeated visits to production wells and midstream infrastructure that accounted for 93% of gas production and 96% of oil production in their study area. The Insight M survey detected 1985 methane emission incidences from 958 distinct sources.

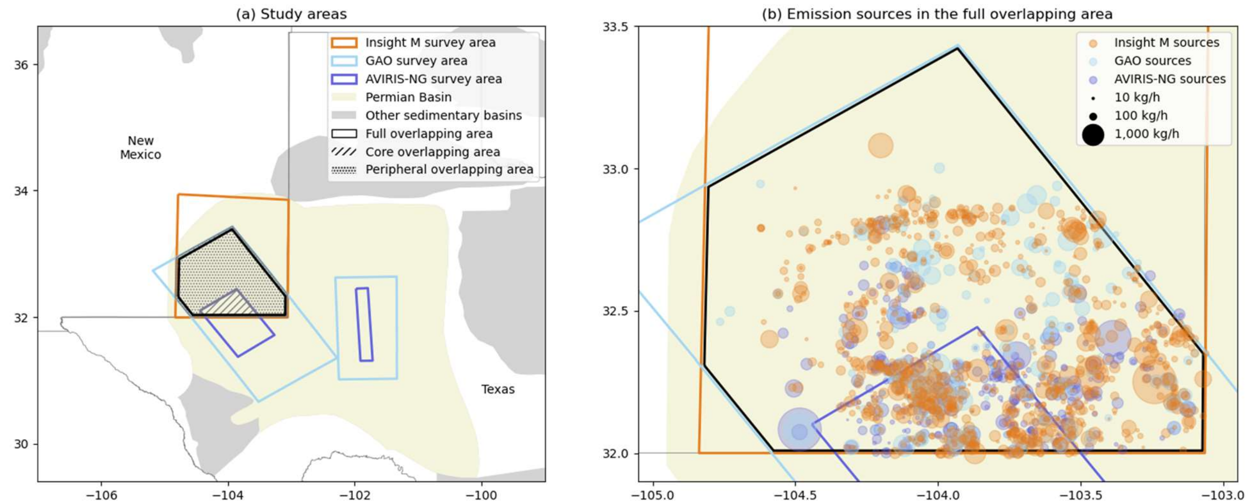

Figure 1. **Study areas and emission sources of the Cusworth et al. survey and the Insight M survey.** (a) Cusworth et al. used the next-generation Airborne Visible/Infrared Imaging Spectrometer (AVIRIS-NG) and the Global Airborne Observatory (GAO) to survey the purple polygons at least 7 times and the light blue polygons at least once, respectively. Insight M surveyed the New Mexico Permian basin 4 times on average (orange polygon). We refer to the intersection of AVIRIS-NG and Insight M survey areas as the "core overlapping area" and the intersection of GAO and Insight M survey areas as the "full overlapping area." The area that is within the full but not the core overlapping area is referred to as the "peripheral overlapping area." Map revised from (Chen, Sherwin *et al* 2022). State boundaries from (U.S. Census Bureau 2018) and sedimentary basin from (U.S. Environmental Information Administration 2020). (b) In the full overlapping area, the Insight M survey found 1856 methane plumes from 893 emission sources. Cusworth et al. survey detected 1258 emission incidences from 607 emission sources. AVIRIS-NG primarily surveyed the core overlapping region and it made some observations in the peripheral overlapping area. Dot sizes show the persistence-weighted emission source sizes.

These two surveys are similar in the sense that 1) they both use airborne hyperspectral imaging to map point sources across large regions, and 2) they are both repeated comprehensive surveys of the oil and gas infrastructure in their study areas (>90% in the Insight M survey and nearly 100% in the Cusworth et al. survey). Thus, the total emissions in the overlapping study area estimated from the two surveys should be similar under the following assumptions: 1) the hyperspectral sensors are similar in performance, 2) measurements were made during similar times and emission levels in the overlapping study area are stable, 3) samples are spatially representative of the overlapping study area, and 4) the sample sizes of the two studies are large enough to produce emissions estimates with modest uncertainties.

However, by applying the same basin-wide quantification method to point sources quantified by the two surveys (Chen, Sherwin et al. 2022), emission estimates at a regional level from these two studies differ. The divergence could be caused by (1) differences between the sensors, (2) survey designs and scopes, or

(3) data processing practices. In this study, we explore these factors in detail by utilizing not only the plume sizes but also the survey information and plume metadata from the two studies.

As listed in Figure 2, this work attempts to reconcile the two aerial studies by using two contrasting approaches: (1) harmonizing study designs and scopes (labeled blue) and (2) post-facto adjustment to account for the effects of different study designs and practices (labeled orange).

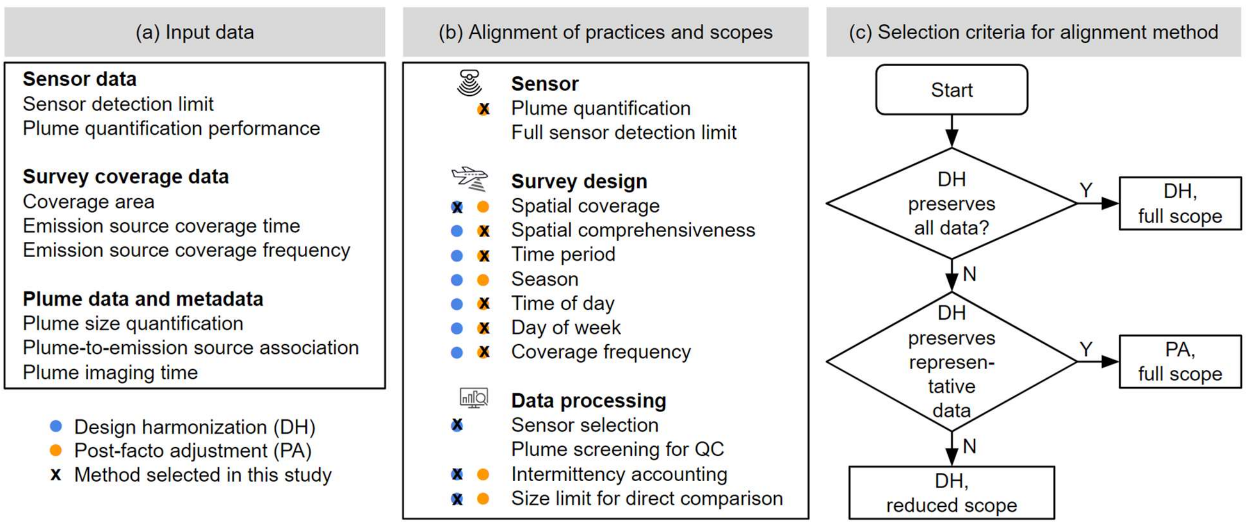

Figure 2. **Input data and steps to align large-scale point source surveys using different sensors, survey designs, and data processing practices.** Direct comparison of emission estimates at a regional level based on different point-source aerial surveys requires alignments of sensor performances, survey designs, and data processing practices. Note that it is not the specific locations of the emission sources, but the survey coverage area that is required as input data for comparing regional aggregate emission estimates. Some aspects can be aligned both through design harmonization (labeled blue) that selects the intersection of the studies for comparison, and through post-facto adjustment (labeled orange) that corrects the results with a factor to account for the discrepancies in the study designs. When both methods are available, we select one of the methods to apply based on their impact on sample size and data representativeness. QC refers to quality control.

In design harmonization, we select the most comparable subset of data at the intersection of the two study designs. Design harmonization generally results in less overall data available for comparison, as only data available from both studies is used, so by definition only a subset of the total data remains usable. For example, by selecting the overlapping geographic area between all studies as the geographic scope for comparison, we reduce the amount of data available, but we achieve better comparability of the results.

In contrast, post-facto adjustment utilizes all available data and imposes correction factors to account for differences in study design. Post-facto adjustment requires enough understanding of the differences in systems to apply reasonable adjustment factors, which is not possible for all types of differences. As an example, post-facto adjustment can be applied to aligning time-of-day effects, where we apply correction factors to “synchronize” surveys conducted at different hours of the day, thus mitigating the discrepancies in emission detection probability across various hours of the day.

For an informal terminology, we have found it helpful to contrast these approaches as being centered on "selecting" or "correcting". That is, we can perform "selecting" by generating a consistent subset (design harmonization) or alternatively we can perform "correcting" to account for differences where possible (post-facto adjustment).

When there is an opportunity to employ either design harmonization or post-facto adjustment, our choice depends on the impact on sample size and data representativeness (Figure 2c). If the application of design harmonization does not result in a significant reduction of sample size, we apply design harmonization. If design harmonization fails to retain sufficient data, we apply post-facto adjustment as long as the subset with design harmonization remains representative of the whole sample. Our criteria for representativeness are twofold: either the subset retains at least 80% of the data, or the post-facto adjustment would not alter the estimates by more than 20%, or approximately one standard deviations of the regional total emissions estimate. If neither criteria is met, we are compelled to use design harmonization, in which case the resulting estimates are only applicable within the subset scope of the original studies after applying design harmonization.

Sensor alignment

As Figure 2 shows, at the sensor level, the two studies may differ in the designs of emission quantification algorithms and the sensor detection limits. In the 2019 Cusworth et al. Permian survey, the imaging spectrometer installed on the GAO aircraft was identical to the AVIRIS-NG instrument (Cusworth *et al* 2021). GAO was deployed at ~5,300 m above mean sea level and surveyed a wider extent of the Permian Basin and the AVIRIS-NG instrument was flown at ~8,500 m to rapidly and repeatedly survey the core production region of the Permian Basin (Cusworth *et al* 2021). Therefore, in theory, the quantification accuracy tested on the GAO should apply similarly for the AVIRIS-NG instrument, but the AVIRIS-NG detection threshold should be higher than that of the GAO due to the greater flight altitude.

Blinded controlled methane release testing is the most reliable way to characterize the quantification performance of a methane sensing system, and can be used to calibrate field measurements (Sherwin, Chen *et al* 2021; Johnson, Tyner, and Szekeres 2021; Rutherford *et al* 2023; El Abbadi *et al* 2023). Controlled releases can also characterize sensors' detection limits. Insight M technology was independently validated single-blind controlled release testings (Sherwin, Chen *et al* 2021; El Abbadi *et al* 2023). The AVIRIS-NG spectrometer was tested with both non-blinded controlled releases (Thorpe *et al* 2016) and blinded controlled releases (Rutherford *et al* 2023; El Abbadi *et al* 2023). In this study, we regard the plume quantifications across sensors reported in Chen, Sherwin *et al* 2022 and Cusworth *et al* 2021 as already aligned based on their controlled release studies. Ideally, all sensors need to be independently validated for this alignment step.

Spatial and temporal alignment

At the study design stage, sampling differences arise due to the spatial differences, temporal differences in sampling, and the underlying sampling variance. Sampling variance is unavoidable and caused by the temporal variation and the intermittency of emissions.

Spatially, different geographic areas may have different emission-relevant quantities such as production intensity, and density of production and midstream infrastructure. We first align the two studies spatially by only comparing emissions found in the overlapping areas (see Figure 1). We divide the full overlapping area into core and peripheral overlapping areas (Figure 1) because AVIRIS-NG primarily covered the core overlapping area. Thus, emissions in the core and peripheral overlapping areas are individually assessed by area and by sensor. The core overlapping area has high well density and production intensity and accounts for about half of the total production in the full overlapping area, though it represents 15% of the spatial area. See the SI, Section S4 for oil and gas production rates.

Spatial comprehensiveness should be considered for comparing survey results. Cusworth et al. performed a comprehensive survey that nearly covered all infrastructure in the survey area at least once. The Insight M survey covered 92% of the active wells in the full overlapping area (96% in the core overlapping area and 89% in the peripheral overlapping area). At the time of the survey, Insight M covered 95% of the gas production in the full overlapping area (98% in the core overlapping area, and 91% in the peripheral overlapping area). We normalize total emissions by the percentage of covered gas production by assuming that both upstream and midstream emissions scale linearly with gas production (e.g., directly observed core overlapping area emissions are grown by a correction factor of 1/0.98 to account for 98% covered production).

Production and emission activities fluctuate significantly over the lifespan of a facility (Cardoso-Saldana and Allen 2021). Emissions can change over long time periods (years) as drilling occurs and depletion sets in at existing wells. Over shorter time periods, production and emissions can fluctuate over the course of seasons, months, days, and even hours.

First, we assess long-running changes in production which might drive changes in emissions. The Permian Basin was the fastest-growing oil and gas-producing basin in the US and we cannot assume stationary production and emissions. Figure 2 shows that time period can be aligned both through design harmonization and post-facto adjustment. Since the Insight M survey period fully encompasses the Cusworth et al. survey period, the design harmonization method would require selecting Insight M data collected within the Cusworth et al. survey period. However, this approach is not viable since Insight M survey coverage in each given month is not evenly distributed over space, meaning that temporally segmenting the Insight M survey introduces significant spatial segmentation and misalignment. See the SI, Section S5 for details.

To avoid using a spatially unrepresentative sample of the Insight M study, and to recognize that the post-facto adjustment introduces less than 20% changes to the emissions estimate, we use the post-facto adjustment method to account for changes in production levels. We normalize total emissions by natural gas production during each survey period. We find total gas production during the Cusworth et al. study period to be 10% more than production during the duration of the Insight M survey. This results in multipliers of approximately 90% applied to Cusworth et al. measured emissions. Alternative normalization based on total energy (oil and gas) production is available in the SI, Section S4.

At smaller time scales of months and seasons, non-uniform production and/or operations might drive non-uniform emissions. However, we cannot quantitatively evaluate seasonality or monthly-scale effects in this study because the 2019 Cusworth et al. survey spanned only 44 days. Satellite data of more frequent coverages can be used to explore seasonality effects (Varon *et al* 2023); however, a detailed comparison to other remote sensing platforms is beyond the scope of this study.

On even smaller scales of days and hours, fluctuations in operations over the course of days or hours could affect emissions. For example, if drilling or maintenance is focused on certain days (e.g., preferentially avoiding weekends) then emissions could be higher on different days. Also, daytime maintenance events can drive emissions higher (though in this study both airplanes utilize daylight measurements).

With regard to days of the week, Insight M surveyed only weekdays and Cusworth et al. surveyed both on weekdays and weekends. We find no significant difference in probabilities of detecting emissions on weekdays and weekends based on the Cusworth et al. survey results, so we do not apply corrections for day-of-week effects. See the SI, Section S2.3 for emission detection probabilities on weekdays and weekends.

Time-of-day effects are evident in the Insight M New Mexico Permian survey. A higher probability of detecting emissions per well visit is found in the morning hours than in the evening hours (Chen, Sherwin *et al* 2022), possibly due to higher levels of maintenance and other operational activity occurring in the morning in the Permian Basin. The same is found with the Cusworth et al. survey, despite more favorable illumination conditions around noon than in the morning for ease of plume detection. We account for the time-of-day effects by aligning the temporal distribution of measurements over the day. See the SI, Section S2.2 for emission detection probabilities at different hours of the day and description of the time-of-day alignment method.

Next, we infer sampling variance through analysis of coverage frequency. For example, if a survey contains only one visit to each asset in the study area, then emissions for a source would have a small uncertainty range that reflects only the quantification noise but not the temporal variation of emissions from each source. The unrealistically small uncertainty range would be an artifact of lacking repeated observations in the simulation. In our compared studies, multiple visits to the same site allow for understanding of temporal variation. In the core overlapping area of our study, the average number of visits to each well (n) ranges from 1.7 (GAO) to 13.5 (AVIRIS-NG + GAO). The AVIRIS-NG + GAO dataset with an average of 13.5 repeated visits gives us an opportunity to demonstrate the abovementioned artifact in the uncertainty range derived from 1.7 GAO visits.

There are two methods to compute the effect of sampling variance. The first method is a directly data-based one. For each asset visited, we may sample x times with replacement from all y observations of the asset in the AVIRIS-NG + GAO dataset, x and y being the number of visits to that particular asset in the GAO and the AVIRIS-NG + GAO dataset. With repeated sampling, this bootstrapping exercise answers to the question of "what the uncertainty range would be if AVIRIS-NG + GAO made the same number of visits as GAO did to each asset?" With more variance in observations in the AVIRIS-NG + GAO dataset, the resulting uncertainty range would be much larger than that of the range based on GAO data only. The other method provides a less precise but simpler solution. The derivation of the uncertainties from fewer observations is analogous to calculating the standard error (*SE*) of a sample mean from a smaller sample. By decreasing the number of visits (n) to each asset, the standard error of the mean emissions shall grow with the square root of n, assuming normally distributed errors. In other words, the uncertainty range from 1.7 visits can be estimated by applying a factor of $\sqrt{13.5/1.7}$ to the uncertainty range estimated with 13.5 AVIRIS-NG + GAO visits, assuming spatially even sampling. This will make the uncertainty range wider than the original range based on 1.7 GAO visits. In this way, the uncertainties of studies with different n can be aligned. We regard this alignment step also as a post-facto adjustment step because the uncertainties from studies of smaller n are corrected based on uncertainties from studies of larger n. We apply both methods below and compare the results.

Data processing alignment

After methane emissions data are collected and attributed to point sources, emission quantification practices may differ in sensor selection at the data processing stage. All sensors employed in the Insight

M survey are identical and identically deployed. The Cusworth et al. survey used two identical sensors mounted on two different platforms (GAO and AVIRIS-NG) for sub-domains of the survey area. GAO and AVIRIS-NG made measurements at different flight altitudes, thus varying the detection thresholds of the sensors mounted on them. In the core overlapping area, we present separate results for each single sensor: Insight M, GAO, and AVIRIS-NG. For the peripheral overlapping area, we only present results by Insight M and GAO, since AVIRIS-NG did not cover it extensively. We also combine GAO and AVIRIS-NG results to estimate emissions based on the whole Cusworth et al. study for core, peripheral, and full overlapping areas.

Another modeling factor is the treatment of emissions below the full detection threshold. The full detection threshold is the theoretical emission rate where the surveying system has a ~100% chance of seeing an emission source larger than the threshold. Below the full detection threshold, the probability of seeing an emission source decays from 100% to 0% as the emission source becomes smaller.

The full detection threshold will vary between the surveys due to the different altitudes of collection, as well as various other possible collection, deployment, sensor, and data processing chain factors. We therefore define a minimum emission rate threshold, or a "size limit for direct comparison" (SLDC). The SLDC ensures a comparable population of very large, ultra-emitter emission sources across all three sensors which we can be confident that the emissions source would reliably be seen by all three sensors.

Due to the sub-selection inherent in this correction, we cannot say that the results are comparable *overall*, but instead that results are comparable for all events above the size threshold. Furthermore, this solution is not ideal as it removes a significant number of detections from the datasets (where systems with higher sensitivity have more data removed) and decouples the final result from a true measure of quantified methane intensity for the given geographic area. Instead, remaining analysis must focus only on methane lost from this subset of sources above the SLDC.

In this study, we estimate the ultra-emitter SLDC using field data collected by AVIRIS-NG, which was the least sensitive deployment due in part to its high altitude of collection. To estimate the SLDC, we assume that the true underlying frequency of emission sources monotonically decreases with emission sizes, such that an emission event of size $2x$ is less frequent than an event of size x, for all x relevant to the study sensors. Under this assumption, a deployed sensor can be assumed to be missing sources when the number of detections drops as we move to smaller plumes. In Figure S2, the peak detection frequencies of Insight M, GAO, and AVIRIS-NG are provided, with AVIRIS-NG having the highest peak frequency for the bin of 316 to 398 kg/h. This represents a minimum emission rate where we expect all sensor deployments to achieve a detection.

We conservatively round up to 500 kg/h, which is approximately the upper limit of the next bin from 398 to 501 kg/h, for our final SLDC. At this rate of 500 kg/h, all three deployed systems are assumed to see all emissions at and above this size within a safe margin. Despite this very high threshold, due to the heavy-tailed distribution of emission sizes, emissions above the SLDC account for most of the total point-source emissions on a mass basis.

Note that this modification results in a significantly smaller absolute estimate of emissions and is no longer representative of an overall regional estimate, due to removing various portions of the dataset through design harmonization. This is permissible in this study because we are not concerned with producing a regional methane intensity estimate nor quantifying the overall volume of emissions, but with comparison and reconciliation of detected emissions in a most directly comparable subset of observations.

Lastly, we observe that persistence is defined differently in the two studies. Insight M computes persistence "by-incidence," treating each measurement as independent, and Cusworth et al. computes "by-day," aggregating all measurements of a given asset conducted on the same day (Equation 1 and 2, respectively). The by-day method applies "or" logic to detection: if two measurements are made on a day, seeing leakage on either measurement 1 *or* measurement 2 would both cause a positive emission event. If a source does not change its state of emissions within each day of survey, the two methods will produce the same persistence estimate. The by-day persistence computed with Equation 2 has the capacity to produce higher persistence than Equation 1 because the by-incidence method takes into account the no-emission detection incidences observed during the days with observed emissions, compared with the "or" logic in the by-day model. We align the studies using design harmonization by applying the "by-incidence" method to both studies. This divergence can also be accounted for by applying an *ad-hoc* correction factor derived from the by-day and by-incidence persistence computed with these studies. However, the design harmonization method is superior here, as it achieves better alignment and does not result in a smaller sample size.

$$Persistence_{incidence} = \frac{Number\ of\ methane\ plumes}{Number\ of\ coverages\ of\ the\ emission\ source} \quad \text{(Equation 1)}$$

$$Persistence_{day} = \frac{Number\ of\ days\ with\ detected\ metha\ \ \ plumes}{Number\ of\ days\ with\ coverages\ of\ the\ emission\ source} \quad \text{(Equation 2)}$$

Design harmonization and post-facto adjustment

Table 1. **Percentage of data preserved through design harmonization (DH) of each alignment step**. If the selected alignment method is post-facto adjustment (PA), alignment factors are applied to the study of the instrument that does not cover the full scope. I, C, G, and A respectively stand for surveys done by Insight M, Cusworth et al. (AVIRIS-NG + GAO), GAO, and AVIRIS-NG.

Alignment of practices and designs	%Data preserved with design harmonization [1]				Selected alignment method	% Change in mean emission estimate with post-facto adjustment [2]			
	I	C	G	A		I	C	G	A
Spatial coverage	16%	46%	17%	61%	DH, reduced scope	N/A			
SLDC	12%	37%	29%	38%	DH, reduced scope				
Intermittency accounting	100%	100%	100%	100%	DH, full scope				
Spatial comprehensiveness	100%	98%	98%	98%	PA, full scope	+2%	-	-	-
Time period	15%	100%	100%	100%	PA, full scope	-	-10%	-10%	-10%
Time of day	94%	97%	100%	96%	PA, full scope	-	+10%	+9%	+13%
Day of week	100%	67%	60%	68%	PA, full scope	+0%	-	+0%	+0%

Notes: [1] Share of data preserved with design harmonization is defined differently for each alignment step. For spatial coverage, time period, and time of day, share of data preserved is defined as the share of remaining well visits associated with the intersection of the two study designs. For size limit for direct comparison (SLDC), data preservation is defined as the share of plumes that is above SLDC. For intermittency accounting, design harmonization shifts the data processing method without causing any data loss. [2] If design harmonization is selected as the alignment method, then we do not need to impose a post-facto correction factor. "-" means that the study already covers the entire scope for comparison (e.g. all assets in the study area, all months during the time period for comparison, and all days of week) and no post-facto correction factor is needed to account for the differences in the survey scope and the comparison scope.

We select an appropriate alignment method for each step, deciding between design harmonization and post-facto adjustment based on their impacts on sample size and data representativeness. As shown in Figure 2, we apply design harmonization by default if it does not reduce sample size. In the case of aligning intermittency accounting, design harmonization causes no data loss and is therefore selected as the alignment method for this step. For all other alignment steps, design harmonization fails to preserve all data. In particular, the data preserved at the intersection of spatial coverages (core overlapping area) and above the SLDC of 500 kg/h each greatly reduces the amount of emissions to be compared. However, it is not feasible to apply post-facto alignment in these cases without more information. Spatial representativeness, time period, time of day, and day of week effects are aligned with post-facto alignment, because the intersected data sufficiently represents the remaining scope. As Table 1 shows, the adjustment factors of all post-facto correction steps do not exceed 20%, suggesting data representativeness and viability of post-facto correction to the entire remaining scope of emissions above the SLDC of 500 kg/h in the core overlapping area.

The order of the alignment steps matters, because the post-facto correction factors depend on the scope of the study for comparison. Design harmonization steps that reduce the scope need to be carried out first. The order of applying the remaining post-facto adjustments is interchangeable and the post-facto alignment steps have multiplicative impacts on the regional emission estimates.

Results

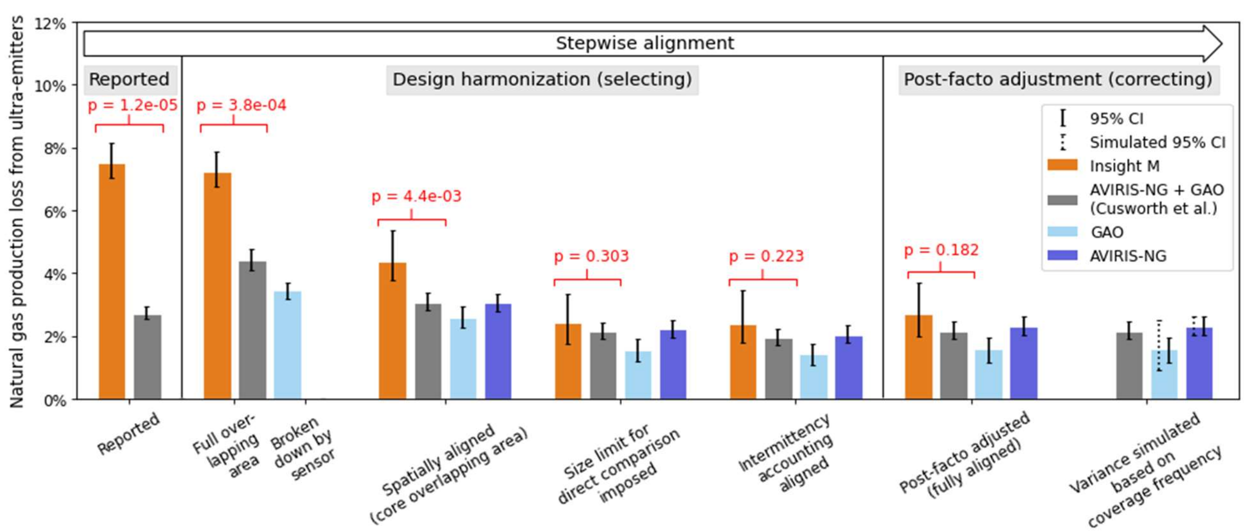

Figure 3. **Stepwise alignment.** Bars reflect reported natural gas production losses. With each movement towards the next set of bars on the right, we apply an additional alignment step. We first apply design harmonization which 1) limits the scope of the comparison to the full overlapping study area and further to the core overlapping area, 2) removes emissions from plumes sized below the size limit for direct

comparison of 500 kg/h, and 3) aligns the intermittency accounting method. Then we apply post-facto adjustments to correct for differing spatial comprehensiveness, time period, time-of-day, and day-of-week effects. The p-values suggest insignificant difference between the Insight M and the Cusworth et al. surveys after full alignment (second set of bars from the right). Error bars show 95% uncertainty ranges from Monte Carlo runs, except that dashed error bars of the rightmost set of bars are simulated with results from the AVIRIS-NG + GAO case based on coverage frequency.

Figure 3 shows stepwise alignments in the order of the alignment steps listed in Table 1. The leftmost bars show the raw reported natural gas production loss of 7.5% (+0.6%/-0.5%) and 2.7% (+0.2%/-0.2%) for the full scope of Insight M and the Cusworth et al. studies. In the full overlapping area, Insight M data leads to an emission estimate of 142 (+12/-9) t/h of methane, by applying the by-incidence persistence accounting method in (Chen, Sherwin *et al* 2022). Applying a similar method to the Cusworth et al. data with default by-day persistence accounting results in an emission estimate of 72 (+8/-9) t/h, 50% lower than the Insight M estimate. These methane emissions estimates correspond to 7.2% (+0.6%/-0.5%) and 3.6% (+0.4%/-0.3%) of methane in natural gas production in the full overlapping area. We evaluate the discrepancies with p-values from two-sided t-tests of the emission estimates with Insight M and Cusworth et al. data. As shown in Figure 3, simple alignment to the full overlapping area increases the p-value from 1.2×10^{-5} to 3.8×10^{-4}, narrowing the discrepancy.

We then break down the Cusworth et al. dataset by sensor (GAO and AVIRIS-NG). Figure 3 does not show AVIRIS-NG results for the full overlapping area because the AVIRIS-NG survey primarily covered the core overlapping area. The AVIRIS-NG + GAO (Cusworth et al.) results include some AVIRIS-NG measurements in the peripheral overlapping area close to the border of the core and the peripheral overlapping areas.

Reducing the scope to the core overlapping area brings the p-value up to 4.4×10^{-3}. It is only in the core overlapping area where we can compare emission estimates based on data collected from all sensors. The core overlapping area accounts for about 54% of the gas production in the full overlapping area and 31% to 42% of the measured emissions (see the SI, Section S3 and S4). This suggests heterogeneous emission intensity across regions and productivities.

We also evaluate only emission sources above the SLDC at 500 kg/h. With a smaller detection threshold (Figure S2), Insight M saw more emissions below SLDC than GAO and AVIRIS-NG, and therefore had more emissions removed at this stage. Thus, this alignment step brings the observations of the two studies closer. The p-value is 0.303 for the reduced scope of emissions above SLDC in the core overlapping area, suggesting statistically insignificant differences in the emission estimates. In other words, when we compare spatially aligned emissions in a size range both technologies can reliably detect, the apparent difference between emissions intensities derived from the two surveys essentially disappears. The remaining alignments are thus conducted as robustness checks.

Aligning the persistence accounting methods brings larger divergence in the estimates. Switching the persistence accounting method from “by day” to “by incidence”, emission estimates based on Cusworth et al. data decrease by approximately 10% and the difference between studies remains statistically insignificant.

Next, to account for the varying survey times, we normalize the studies by the natural gas production at the times of the surveys. The Permian Basin grew in gas production during the Insight M survey time.

The gas production rate in the core overlapping area is 10% higher during the Cusworth et al. survey time than the Insight M survey time. Assuming a proportional change in emissions with respect to gas production, we adjust the Cusworth et al. emissions down by 10% to simulate temporal alignment. We present an alternative method of normalization with overall energy production (oil and gas) in the SI, Section S4.

The Insight M survey was on average conducted at earlier times of day than the AVIRIS-NG and the GAO survey, increasing the probability of detecting emissions compared with later times (see the SI, Section S2.2). We align the surveys to have a similar distribution of measurements by time of day by applying a factor of 1.13 to the AVIRIS-NG results, 1.09 to GAO results, and 1.10 to the Cusworth et al. results (Table 1).

Lastly, we normalize by the comprehensiveness of the surveys, scaling up estimated emissions to account for assets in the survey area that were not measured. In this step, the Insight M estimate increases by 2% to account for emissions from production that were not covered in the core overlapping area.

Figure 3 shows the aggregated impacts of the abovementioned post-facto adjustment steps. P-value after this step is 0.182, which is not statistically significant after imposing all of the above alignment steps. The relative difference, defined as the absolute difference in the mean ultra-emitter loss estimates from the Insight M study and the Cusworth et al. study divided by the Cusworth et al. ultra-emitter production loss, goes down from 176% in raw reported values to 13% in the fully aligned results.

The fully aligned and directly comparable ultra-emitter emissions in the core overlapping area are estimated to be 26 (+11/-7) t/h by Insight M, 17±4 t/h by GAO, 25±3 t/h by AVIRIS-NG, and 23±3 t/h by Cusworth et al. (AVIRIS-NG + GAO). These emissions, limited to those released at or above rates of 500 kg/h and therefore representing a fraction of what were detected by these systems in this area, respectively correspond to 2.4% (+1.0%/-0.7%), 1.6%±0.3%, 2.3%±0.3%, and 2.2%±0.3% of the natural gas production in the area. Despite the varying quantification algorithms across sensors and unalignable aspects such as plume screening practices, the aligned results show agreement within statistical errors for emissions above SLDC in the core overlapping area, with the exception of GAO.

This is possibly due to the low coverage frequency by GAO, which causes under-representativeness of ultra-emitters sized over 1000 kg/h in the GAO dataset, as demonstrated in Figure 4 and the Discussion section. Another factor contributing to the disparate findings by the GAO is the unrealistically narrow uncertainty ranges stemming from an artifact in the Monte Carlo simulation in estimating uncertainties with insufficient repetitions of observations.

We demonstrate this artifact by adjusting the width of the error bars in Figure 3. In the core overlapping area, the average number of visits to each well (n) ranges from 1.7 (GAO) to 13.5 (AVIRIS-NG + GAO). The first coverage frequency alignment method directly samples x times with replacement from all available AVIRIS-NG + GAO observations of each emission source, x being the number of coverages to the emission source of the study to simulate the uncertainties based on all AVIRIS-NG + GAO data. The sampling indicates that the simulated GAO and AVIRIS-NG error bars are the width of the AVIRIS-NG + GAO error bars grown by a factor of 2.7 and 1.1, respectively. The second alignment method adjusts the uncertainty ranges with the average number of visits to each asset. The leftmost set of bars in Figure 3 demonstrate this effect by treating the AVIRIS-NG + GAO uncertainties based on 13.5 visits as the ground truth. If we reduce n from 13.5 to 1.7, the error bars would grow in width by a factor of $\sqrt{13.5/1.7} = 2.8$, shown as the simulated GAO error bars in Figure 3. The simulated AVIRIS-NG error bars are similar to the original ones because the factor of $\sqrt{13.5/11.8}$ is close to 1. The two methods yield similar results in simulated error bars. We do not show an adjustment of the Insight M error bars based on Cusworth et al. results, recognizing the difference in their sensor performances and survey designs. By correcting for the uncertainties, we show widened GAO error bars overlapping with the uncertainty ranges of the Cusworth et al. results. We further demonstrate the impact of coverage frequency in Figure 5 and the Discussion section.

Discussion

Size limit for direct comparison (SLDC)

Figure 4 shows fully aligned emission rates for all subregions defined in Figure 1. We show total emissions as a function of the value selected for the SLDC (set as 500 kg/h in the analysis above). The studies are temporally aligned to Insight M survey time, time-of-day aligned to Insight M survey hours, spatial comprehensiveness aligned to be fully comprehensive, and persistence accounting aligned to the "by-incidence" method.

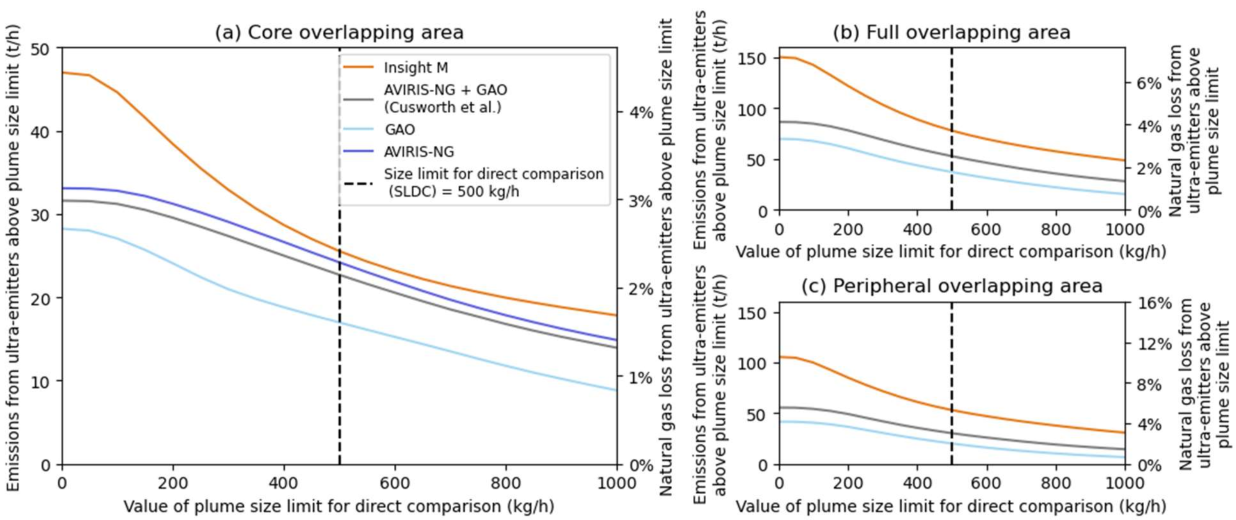

Figure 4. ***Aligned total* emissions from observations in the (a) core, (b) full, and (c) peripheral overlapping areas.** The results are temporally aligned to Insight M survey time, time-of-day aligned to Insight M survey hours, spatial comprehensiveness aligned to be fully comprehensive, and persistence accounting aligned to the "by incidence" method. We do not show purple lines for AVIRIS-NG in (b) and (c) because AVIRIS-NG did not survey the peripheral overlapping area extensively.

The fully aligned results in Figure 3 correspond to the emissions at an SLDC of 500 kg/h in Figure 4a. Below 500 kg/h, Insight M detected more emissions due to its lower detection limit (more than half of the total detected emissions by Insight M came from sources below this 500 kg/h threshold). GAO detected more emissions than AVIRIS-NG due to its lower flight altitude.

Notably in Figure 4a, the slopes of all four curves in the 500 to 1000 kg/h range are similar, suggesting similar amount of methane detected in this range. The discrepancies are mostly in methane detected from plumes sized over 1000 kg/h, shown by the differing levels of intersection of the curves with the right yaxis. Such discrepancy is much more apparent in the GAO survey not only in the core overlapping area but also in the full and peripheral overlapping areas (Figure 4b and 4c), possibly due to GAO's lower coverage frequency that failed to detect as many super-emitting events over 1000 kg/h as detected by Insight M and AVIRIS-NG. We expect this as one probable reason why the fully aligned GAO bar in Figure 3 is lower. Without AVIRIS-NG data in the full and peripheral overlapping areas, Cusworth et al. results largely depend on GAO data that exhibit large discrepancies from Insight M results in terms of emissions above 1000 kg/h.

Robustness checks

As shown in Figure 3, when we limit the scope of the comparison to emissions detected in the core overlapping area from plumes sized over the SLDC of 500 kg/h, the p-value increases to 0.303 and the differences between emissions intensities derived from the Insight M and the Cusworth et al. surveys essentially disappear. The remaining alignments, including alignments for intermittency accounting, spatial comprehensiveness, and temporal differences, can thus be viewed as robustness checks.

Section S3.1 in the SI details the impact of each remaining alignment step. Aligning the intermittency accounting methods brings down Cusworth et al. emissions by 7.8% to 9.8%. The overall effects of all post-facto correction steps are respectively +2%, -1%, -2%, and +2% for Insight M, Cusworth et al., GAO, and AVIRIS-NG.

To conclude, all remaining robustness check steps introduce less than 10% changes to the estimates derived in the results after simply imposing spatial alignment and SLDC. Therefore, steps for limiting the scope of comparison to the most comparable subset are the most important alignment steps in this reconciliation study.

Importance of repeated survey

Why does GAO see fewer emissions above 1000 kg/h (Figure 4)? One probable explanation for the remaining discrepancy is the coverage frequency. As discussed in Chen, Sherwin *et al* 2022, large sample sizes are essential for capturing the low-frequency high-impact super-emitters. Comprehensive surveys are key for collecting such large sample sizes. However, due to the intermittent nature of many emission sources, the degree to which one comprehensive survey can capture enough of the heavy tail and characterize the heavy-tailed distribution requires further investigation.

As a demonstration, we use AVIRIS-NG data over repeated visits to show the impact of coverage frequency on the estimate of the regional total emissions. AVIRIS-NG made an average of 11.8 visits to 3,498 wells in the core overlapping area, finding 319 distinct emission sources. From these 319 sources, we pick 311 that were covered at least on 8 days by AVIRIS-NG. We then use the first observation of the first 8 observation days of these 311 emission sources for simulating uncertainties from repeated visits (Figure 5a). In this simulation exercise, we include emissions below the SLDC of 500 kg/h.

With all 8 AVIRIS-NG observations, the mean total emission from these 311 sources is 31.0 t/h. If, for each emission source, we sample with replacement the 8 observations 8 times to simulate 8 comprehensive surveys, then the standard error of mean (*SE*) is estimated at 1.8 t/h. *SE* declines with the square root of the number of observations until the survey becomes uncomprehensive.

Note that the simulated *SE* values are underestimates for two reasons: 1) the simulation assumes that 8 times of observations fully capture the underlying distribution, whereas it is possible that the true variance is larger, and 2) the simulation assumes independence between observations. However, observations made on the same day can have significant correlations. If instead, we produce 8 AVIRIS-NG snapshots based on same-day observations, the estimated total emissions from the 311 sources range from 19.0 to 49.1 t/h (dotted lines in Figure 5a), suggesting a wider 95% confidence interval of mean emission estimates that the interval with one simulated comprehensive survey assuming independence between observations (blue bar in Figure 5a).

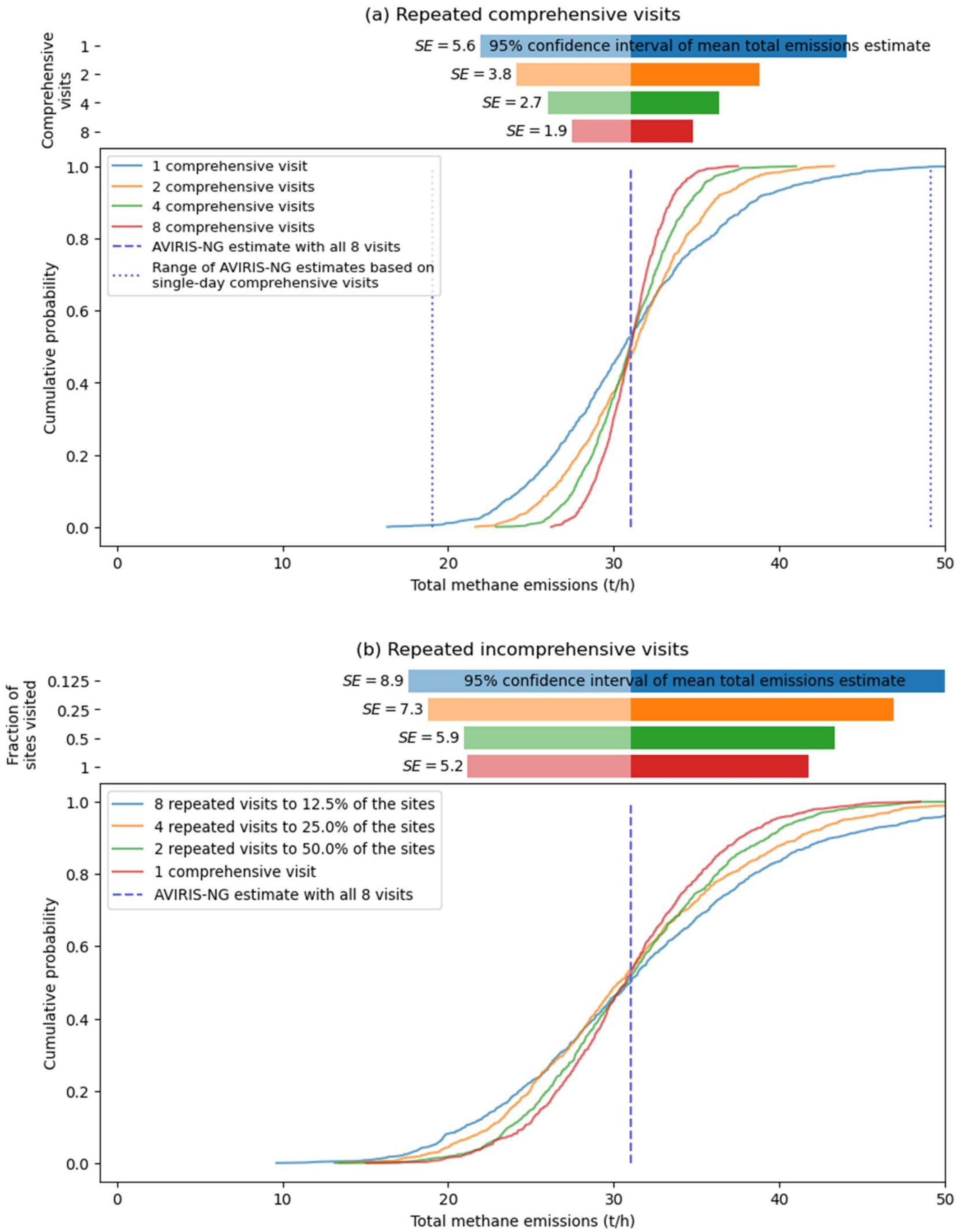

Figure 5. **Standard error of mean of regional emission estimates using (a) 1 to 8 AVIRIS-NG visits to 311 emission sources in the core overlapping area, and (b) 311 visits to 12.5% to 100% of the 311 emission sources.** The CDF curves show simulated mean methane emissions estimate with 1000

iterations. The top bars show the 95% confidence intervals of the mean and are annotated with standard error of mean (SE). This simulation assumes independence between observations. A wider range of same-day AVIRIS-NG estimates (dotted lines) than the 95% confidence interval of mean emission estimates with one comprehensive survey (red bar), suggests correlation between observations made on the same day. (b) shows that if an operator has the resource to deploy one comprehensive visit to 311 potential emission sources, then making one comprehensive survey results in smaller *SE* in extrapolated total emissions than making repeated surveys to a subset of emission sources.

On the day when AVIRIS-NG detected 19.0 t/h from the 311 emission sources, 15.9 t/h was from plumes larger than 500 kg/h, rendering the possibility that GAO saw 17±4 t/h of emissions above that size limit in the core overlapping area. 99% of GAO observations in the core overlapping area were made on two different days.

The other set of simulations ran with the 8 AVIRIS-NG observations are repeated less-than-comprehensive surveys (Figure 5b). If given the flight time to cover all 3,498 wells in the core overlapping area, one may choose to do one comprehensive survey or repeated uncomprehensive surveys to a fraction of the assets. We test 1, 2, 4, and 8 repeated surveys with the same number of total well visits, assuming the frequency of emission events is homogeneous across all assets. The simulation shows that to estimate the mean total emissions from all sites of interest, one comprehensive survey gives the smallest *SE*. This result suggests stronger spatial variation than temporal variation in emissions in this area, and therefore that it is more useful for uncertainty reduction to capture all sites than to visit the same sites repeatedly. Future flight campaigns intended to characterize regional emissions with similar aircraft platforms should be designed to evenly cover the entire area of interest to achieve lower *SE* of regional emissions estimate.

Subregional differences

Figure 4 shows larger emissions across sensors in the peripheral overlapping area than in the core overlapping area, despite similar total gas production in these two subregions (see the SI, Section S3). The most obvious subregional difference in emissions is the larger share of midstream emissions in the peripheral overlapping area. Figure 6a breaks down the emissions by source types in the two subregions. Note that there are slight differences in the definition of source types by the Chen, Sherwin et al. study and by Cusworth et al. Chen, Sherwin, et al. categorize tanks on well-sites as well-site emissions and Cusworth et al. categorize tank-on-well-site emissions as tank emissions. The tank category by Chen, Sherwin et al. refers to stand-alone sites with just tanks and no other equipment such as wellheads and compressors. Therefore, it is more robust to compare the grouped upstream emissions from wells, tanks, and compressor stations from the two studies.

To better demonstrate subregional differences, all plume data, including plumes below the SLDC of 500 kg/h are presented in this section. The contribution of midstream emissions is evident in the gridded natural gas production loss estimates (detected emissions in a gridded "pixel" normalized by with methane produced in that pixel) in Figure 6b and 6c. Some pixels in these maps have high production normalized loss rates (over 100% in some cases), which implies significant midstream emissions in the pixel or incompleteness of the production dataset.

Moreover, both the Insight M and the Cusworth et al. study estimate larger emissions from well sites (note that this includes some "storage tank" emissions in the Cusworth et al. study due to its definition) in the lower-productivity peripheral overlapping area than in the high-productivity core overlapping area, an observation consistent with findings of significant emissions from low productivity well sites (Omara *et al* 2022).

The subregional differences in emission intensity are significant. Although the core overlapping area is more production-intensive, it is less emission-intensive in terms of emissions normalized to production. If an aerial survey comprehensively covers all assets in a part of the basin that is the most production-intensive, it still misses the large midstream emissions in the peripheral region of lower productivity. Therefore, the conclusions based on the sub-basin level survey should be confined to the survey area and cannot be reliably extrapolated to the full basin. This dependence of loss rate on asset productivity is similar to that seen in (Omara *et al* 2022, Rutherford *et al* 2021,) among others. (Sherwin *et al* 2024) illustrates that the Cusworth et al. data leads to production losses of respectively 3.4%±0.2% and 8.5%±0.8% in survey areas in the Delaware Sub-basin and the Midland Sub-basin, where Delaware is significantly more productive than the Midland.

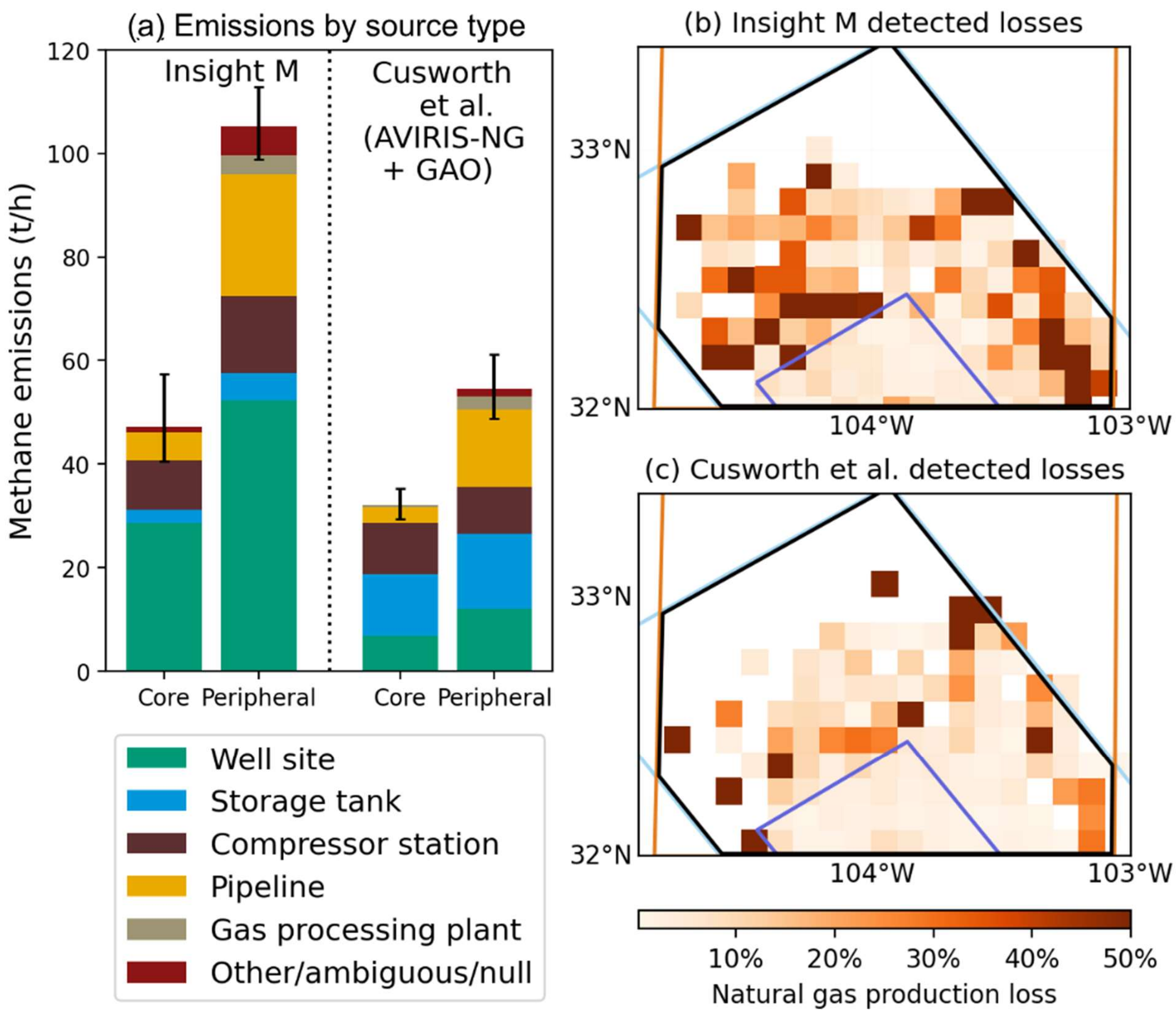

Figure 6. **Subregional differences in emissions.** (a) Both the Insight M survey and the Cusworth et al. (AVIRIS-NG + GAO) survey reveal larger shares of emissions from pipelines and gas processing plants in the peripheral overlapping area than in the core overlapping area. Note the differences in the definition of source types by the two studies. Cusworth et al. categorize tank-on-well-site emissions as tank

emissions, and the Insight M tank category refers to stand-alone sites with just tanks and no other equipment such as wellheads and compressors. (b) and (c) are gridded natural gas production loss rates (detected emissions normalized with methane in gross gas production) in the core (enclosed by purple lines) and peripheral (enclosed by blue, purple, and black lines) overlapping areas. The color scale limits at 50% to better show the distribution; some gridded production loss rates are over 100% due to midstream emissions.

Conclusion

We reconcile estimates of basin-wide emissions from large point sources from two aerial surveys with hyperspectral sensors across the New Mexico Permian Basin in 2019. Starting with seemingly divergent results, we identify important aspects that need to be aligned before comparing results from the two studies. After aligning on the subset of most comparable emission sources, the results of the two studies are statistically indistinguishable, with a p-value between emissions estimates of the two studies of 0.182, much greater than the value of 0.05 often used to determine statistical significance. Therefore, this study demonstrates reconcilability in regional methane emission estimates derived by these two hyperspectral studies.

Because they can be deployed at basin or regional scales, aerial surveys are capable of detecting large, rare emissions, and therefore form an invaluable basis for estimating regional emissions. However, as with any measurement, it is necessary to exercise caution when incorporating these datasets into emissions inventories. As this study shows, emission estimates made with aerial surveys may differ due to their varying survey design, sensor capabilities, and data processing practices.

Ensuring spatial alignment is one of the most important steps toward reconciling multiple emissions surveys, and this likely extends to other survey approaches including satellites and ground surveys. This is because emissions variability is strongly driven by production variability. We find that a high-productivity subregion shows lower emission intensity than other areas, and a survey confined to this high-productivity region misses substantial emissions from the lower-productivity peripheral region. Therefore, to infer the total emissions contribution from large point sources, methane surveys should ensure the measured assets are representative of the area of interest both in space and productivity characteristics. Surveys should also not neglect peripheral areas where high emissions intensities (e.g., high fractional loss rates) have been found.

Another important consideration for accurate inference is survey coverage frequency. Due to the heavy-tailed and intermittent nature of the very large emission sources analyzed here, sometimes one comprehensive survey may not achieve the desired level of accuracy, as the variance between the 8 AVIRIS surveys suggests. In cases of inventory development where a high level of accuracy is desired, one may consider repeatedly conducting comprehensive aerial surveys to reduce the standard error of estimated mean emissions.

To conclude, this study provides a basis for comparing comprehensive hyperspectral aerial survey results, and re-confirms the validity of their methane estimates. Future aerial campaigns for measuring basin-wide emissions should consider extending spatial coverage to all assets, and ensuring repeat measurements.

References

Alvarez R A, Zavala-Araiza D, Lyon D, Allen D T, Barkley Z R, Brandt A R, Davis K J, Herndon S C, Jacob D J, Karion A, Kort E A, Lamb B K, Lauvaux T, Maasakkers J D, Marchese A J, Omara M, Pacala S W, Peischl J, Robinson A L, Shepson P B, Sweeney C, Townsend-Small A, Wofsy S C and Hamburg S P 2018 Assessment of methane emissions from the U.S. oil and gas supply chain *Science (80-.).* **361** 186–8

Barkley Z, Davis K, Miles N, Richardson S, Deng A, Hmiel B, Lyon D and Lauvaux T 2023 Quantification of oil and gas methane emissions in the Delaware and Marcellus basins using a network of continuous tower-based measurements *Atmos. Chem. Phys.* **23** 6127–44

Brandt A R, Heath G A and Cooley D 2016 Methane Leaks from Natural Gas Systems Follow Extreme Distributions *Environ. Sci. Technol.* **50** 12512–20 Online: https://pubs.acs.org/sharingguidelines

Chen Y, Sherwin E D, Berman E S F, Jones B B, Gordon M P, Wetherley E B, Kort E A and Brandt A R 2022 Quantifying Regional Methane Emissions in the New Mexico Permian Basin with a Comprehensive Aerial Survey *Environ. Sci. Technol.* **56** 4317–23

Cardoso-Saldana F J and Allen D T 2021 Projecting e temporal evolution of meane emissions from oil and gas production basins *Environ. Sci. Technol.* **55** 2811–9

Conrad B, Tyner D R and Johnson M R Robust Probabilities of Detection and Quantification Uncertainty for Aerial Methane Detection : Examples for Three Airborne Technologies *Remote Sens. Environ.*

Cusworth D H, Duren R M, Thorpe A K, Olson-Duvall W, Heckler J, Chapman J W, Eastwood M L, Helmlinger M C, Green R O, Asner G P, Dennison P E and Miller C E 2021 Intermittency of Large Methane Emitters in the Permian Basin *Environ. Sci. Technol. Lett.* **8** 567–73

Cusworth D H, Thorpe A K, Ayasse A K, Stepp D, Heckler J, Asner G P, Miller C E, Yadav V, Chapman J W, Eastwood M L, Green R O, Hmiel B, Lyon D R and Duren R M 2022 Strong methane point sources contribute a disproportionate fraction of total emissions across multiple basins in the United States *Proc. Natl. Acad. Sci. U. S. A.* **119** 1–7

Duren R M, Thorpe A K, Foster K T, Rafiq T, Hopkins F M, Yadav V, Bue B D, Thompson D R, Conley S, Colombi N K, Frankenberg C, McCubbin I B, Eastwood M L, Falk M, Herner J D, Croes B E, Green R O and Miller C E 2019 California's methane super-emitters *Nature* **575** 180–4

El Abbadi S H, Chen Z, Burdeau P M, Rutherford J S, Chen Y, Zhang Z, Sherwin E D and Brandt A R 2023 Comprehensive evaluation of aircraft-based methane sensing for greenhouse gas mitigation. *Preprint.*

Enverus 2023 Enverus Solutions for Exploration & Production Online: https://www.enverus.com/solutions/energy-analytics/ep/

Frankenberg C, Thorpe A K, Thompson D R, Hulley G, Kort E A, Vance N, Borchardt J, Krings T, Gerilowski K, Sweeney C, Conley S, Bue B D, Aubrey A D, Hook S and Green R O 2016 Airborne methane remote measurements reveal heavytail flux distribution in Four Corners region *Proc. Natl. Acad. Sci. U. S. A.* **113** 9734–9 Online: https://www-pnas-org.stanford.idm.oclc.org/content/113/35/9734

Irakulis-Loitxate I, Guanter L, Liu Y N, Varon D J, Maasakkers J D, Zhang Y, Chulakadabba A, Wofsy S C, Thorpe A K, Duren R M, Frankenberg C, Lyon D R, Hmiel B, Cusworth D H, Zhang Y, Segl K, Gorroño J, Sánchez-García E, Sulprizio M P, Cao K, Zhu H, Liang J, Li X, Aben I and Jacob D J 2021 *Satellite-based survey of extreme methane emissions in the Permian basin* vol 7 Online: http://advances.sciencemag.org/

Johnson F, Wlazlo A, Keys R, Desai V, Wetherley E, Calvert R and Berman E 2021a Airborne methane surveys pay for themselves: An economic case study of increased revenue from emissions control

[Preprint] Online: https://eartharxiv.org/repository/view/2532/

Johnson M R, Tyner D R and Szekeres A J 2021b Blinded evaluation of airborne methane source detection using Bridger Photonics LiDAR *Remote Sens. Environ.* **259** 112418 Online: https://doi.org/10.1016/j.rse.2021.112418

Johnson, M R, Conrad, B M, & Tyner, D R 2023 Creating measurement-based oil and gas sector methane inventories using source-resolved aerial surveys *Nature Communications Earth & Environment* 4(1), 139

Kairos Aerospace *Kairos Aerospace Technical White Paper: Methane Detection* Online: http://kairosaerospace.com/wp-content/uploads/2019/09/Kairos-Aerospace-Methane-Detection.pdf

Lyon D R, Hmiel B, Gautam R, Omara M, Roberts K A, Barkley Z R, Davis K J, Miles N L, Monteiro V C, Richardson S J, Conley S, Smith M L, Jacob D J, Shen L, Varon D J, Deng A, Rudelis X, Sharma N, Story K T, Brandt A R, Kang M, Kort E A, Marchese A J and Hamburg S P 2021 Concurrent variation in oil and gas methane emissions and oil price during the COVID-19 pandemic *Atmos. Chem. Phys.* **21** 6605–26

McNorton J, Bousserez N, Agusti-Panareda A, Balsamo G, Cantarello L, Engelen R, Huijnen V, Inness A, Kipling Z, Parrington M and Ribas R 2022 Quantification of methane emissions from hotspots and during COVID-19 using a global atmospheric inversion *Atmos. Chem. Phys.* **22** 5961–81

MethaneSAT 2023 Data sneak peeks: Case studies from MethaneAIR flights. Online: https:// https://www.methanesat.org/data/

MethaneSAT 2024 MethaneAIR on Earth Engine. Online: https://showcase.earthengine.app/view/methanesat/

New Mexico 2021 *The New Mexico Administrative Code Title 19 Chapter 15 Part 18.* Online: https://www.srca.nm.gov/parts/title19/19.015.0018.html

Omara M, Zavala-Araiza D, Lyon D R, Hmiel B, Roberts K A and Hamburg S P 2022 Methane emissions from US low production oil and natural gas well sites *Nat. Commun. 2022 131* **13** 1–10 Online: https://www-nature-com.stanford.idm.oclc.org/articles/s41467-022-29709-3

Robertson A M, Edie R, Field R A, Lyon D, McVay R, Omara M, Zavala-Araiza D and Murphy S M 2020 New Mexico Permian Basin Measured Well Pad Methane Emissions Are a Factor of 5–9 Times Higher Than U.S. EPA Estimates *Environ. Sci. Technol.*

Rutherford J S, Sherwin E D, Ravikumar A P, Heath G A, Englander J, Cooley D, Lyon D, Omara M, Langfitt Q and Brandt A R 2021 Closing the methane gap in US oil and natural gas production emissions inventories *Nat. Commun.* **12** 1–12

Rutherford J S, Sherwin E D, Chen Y, Aminfard S and Brandt A R 2023 Evaluating methane emission quantification performance and uncertainty of aerial technologies via high-volume single-blind controlled releases. *Preprint.*

Schneising O, Buchwitz M, Reuter M, Vanselow S, Bovensmann H and P. Burrows J 2020 Remote sensing of methane leakage from natural gas and petroleum systems revisited *Atmos. Chem. Phys.* **20** 9169–82

Schwietzke S, Harrison M, Lauderdale T, Branson K, Conley S, George F C, Jordan D, Jersey G R, Zhang C, Mairs H L, Pétron G and Schnell R C 2019 Aerially guided leak detection and repair: A pilot field study for evaluating the potential of methane emission detection and cost-effectiveness *J. Air Waste Manag. Assoc.* **69** 71–88

Shen L, Gautam R, Omara M, Zavala-Araiza D, Maasakkers J D, Scarpelli T R, Lorente A, Lyon D, Sheng J, Varon D J, Nesser H, Qu Z, Lu X, Sulprizio M P, Hamburg S P and Jacob D J 2022 Satellite quantification of oil and natural gas methane emissions in the US and Canada including contributions from individual basins *Atmos. Chem. Phys.* **22** 11203–15

Sherwin E D, Chen Y, Ravikumar A P and Brandt A R 2021 Single-blind test of airplane-based hyperspectral methane detection via controlled releases. *Elem Sci Anth, 9(1), 00063*

Sherwin E D, Rutherford J, Zhang Z, Chen Y, Wetherley E B, Yakovlev P, Berman E S F, Jones B, Thorpe A K, Duren R, Brandt A and Cusworth D H 2024 US oil and gas system emissions from nearly one million aerial site measurements *Nature* **627**, 328–334 (2024)

Thorpe A K, Frankenberg C, Aubrey A D, Roberts D A, Nottrott A A, Rahn T A, Sauer J A, Dubey M K, Costigan K R, Arata C, Steffke A M, Hills S, Haselwimmer C, Charlesworth D, Funk C C, Green R O, Lundeen S R, Boardman J W, Eastwood M L, Sarture C M, Nolte S H, Mccubbin I B, Thompson D R and McFadden J P 2016 Mapping methane concentrations from a controlled release experiment using the next generation airborne visible/infrared imaging spectrometer (AVIRIS-NG) *Remote Sens. Environ.* **179** 104–15

U.S. Census Bureau 2018 US State Boundaries. Online: https://www.census.gov/geographies/mapping-files/time-series/geo/carto-boundary-file.html

U.S. Environmental Information Administration 2020 Sedimentary basins Online: https://atlas.eia.gov/datasets/6542690951ca45f2a3c23a4325153d7d_0/explore

U.S. Environmental Information Administration 2022 The Waha Hub natural gas price continues to fall below the Henry Hub price Online: https://www.eia.gov/todayinenergy/detail.php?id=53919

U.S. Environmental Protection Agency 2023 Overview of Greenhouse Gases Online: https://www.epa.gov/ghgemissions/overview-greenhouse-gases

Varon D J, Jacob D J, Hmiel B, Gautam R, Lyon D R, Omara M, Sulprizio M, Shen L, Pendergrass D, Nesser H, Qu Z 2023 Continuous weekly monitoring of methane emissions from the Permian Basin by inversion of TROPOMI satellite observations *Atmospheric Chemistry and Physics*. 23(13):7503-20.

Zhang Y, Gautam R, Pandey S, Omara M, Maasakkers J D, Sadavarte P, Lyon D, Nesser H, Sulprizio M P, Varon D J, Zhang R, Houweling S, Zavala-Araiza D, Alvarez R A, Lorente A, Hamburg S P, Aben I and Jacob D J 2020 Quantifying methane emissions from the largest oil-producing basin in the United States from space *Sci. Adv.* **6** 1–10

Acknowledgments

We thank Eric Kort of the University of Michigan, Mint Kunkel at Bridger Photonics, and Jack Warren and Alba Lorente at Environmental Defense Fund (EDF) for providing valuable comments on the analysis. We gratefully acknowledge I. Irakulis-Loitxate for providing satellite-derived data to support analysis of detection frequency.

Y.C. and A.R.B. are partially funded by the Alfred P. Sloan Foundation Grant G-2019-12451 in support of the Flaring and Fossil Fuels: Uncovering Emissions and Losses (F3UEL) project.

Funding for Y.C., E.D.S., and A.R.B. was provided by the Stanford Natural Gas Initiative, an industry consortium that supports independent research at Stanford University.

YC receives funding from EDF.

Funding for AVIRIS-NG and GAO flight operations and/or data analysis referenced in this paper was provided by NASA's Carbon Monitoring System and Advanced Information System Technology programs as well as Carbon Mapper, RMI, the Environmental Defense Fund, the California Air

Resources Board, the University of Arizona, and the US Climate Alliance. Portions of this research were carried out at the Jet Propulsion Laboratory, California Institute of Technology, under a contract with the National Aeronautics and Space Administration (80NM0018D0004). The Global Airborne Observatory (GAO) is managed by the Center for Global Discovery and Conservation Science at Arizona State University. The GAO is made possible by support from private foundations, philanthropic individuals, and Arizona State University.

This work is not a product of the United States Government or the United States Environmental Protection Agency (EPA), and the author is not doing this work in any governmental capacity. The views expressed are those of the authors only and do not necessarily represent those of the United States or the US EPA.

Competing interests

The authors declare the following competing financial interest(s): E.S.F.B., P.V.Y., B.B.J., and E.B.W. are employees of Insight M. D.H.C. and RM.D. are employees of the University of Arizona and seconded to the non-profit organization Carbon Mapper. Remaining authors have no competing interests to declare.

Data accessibility statement

Cusworth et al. 2019 Permian campaign data is available at https://pubs.acs.org/doi/10.1021/acs.estlett.1c00173. Insight M New Mexico Permian campaign data is available at https://github.com/KairosAerospace/stanford_nm_data_2021. Code for generating main results and figures are available at https://github.com/yuliachen/Reconciling-methane-emission-estimates-from-two-aerial-surveys-in-the-Permian-Basin.